NeuroImage 211 (2020) 116607

Contents lists available at ScienceDirect

NeuroImage

journal homepage: www.elsevier.com/locate/neuroimage

Cholinergic white matter pathways make a stronger contribution to attention and memory in normal aging than cerebrovascular health and nucleus basalis of Meynert

Milan Nemy [a], Nira Cedres [b,c], Michel J. Grothe [d], J-Sebastian Muehlboeck [b], Olof Lindberg [b], Zuzana Nedelska [e,f], Olga Stepankova [g], Lenka Vyslouzilova [g], Maria Eriksdotter [b,h], José Barroso [c], Stefan Teipel [d,i], Eric Westman [b,j], Daniel Ferreira [b,c,*]

[a] Department of Cybernetics, Faculty of Electrical Engineering, Czech Technical University, Prague, Czech Republic
[b] Division of Clinical Geriatrics, Center for Alzheimer Research, Department of Neurobiology, Care Sciences and Society, Karolinska Institutet, Stockholm, Sweden
[c] Faculty of Psychology, University of La Laguna, La Laguna, Tenerife, Spain
[d] Clinical Dementia Research Section, German Center for Neurodegenerative Diseases (DZNE), Rostock, Germany
[e] Memory Clinic, Department of Neurology, Charles University, 2nd Faculty of Medicine and Motol University Hospital, Prague, Czech Republic
[f] Department of Radiology, Mayo Clinic, Rochester, MN, USA
[g] Czech Institute of Informatics, Robotics, and Cybernetics, Czech Technical University, Prague, Czech Republic
[h] Theme Aging, Karolinska University Hospital, Stockholm, Sweden
[i] Department of Psychosomatic Medicine, University Medicine Rostock, Rostock, Germany
[j] Department of Neuroimaging, Centre for Neuroimaging Sciences, Institute of Psychiatry, Psychology, and Neuroscience, King's College London, London, UK

ARTICLE INFO

Keywords:
Cholinergic system
Basal forebrain
Normal aging
Small vessel disease
Cognition
Magnetic resonance imaging

ABSTRACT

The integrity of the cholinergic system plays a central role in cognitive decline both in normal aging and neurological disorders including Alzheimer's disease and vascular cognitive impairment. Most of the previous neuroimaging research has focused on the integrity of the cholinergic basal forebrain, or its sub-region the nucleus basalis of Meynert (NBM). Tractography using diffusion tensor imaging data may enable modelling of the NBM white matter projections. We investigated the contribution of NBM volume, NBM white matter projections, small vessel disease (SVD), and age to performance in attention and memory in 262 cognitively normal individuals (39–77 years of age, 53% female). We developed a multimodal MRI pipeline for NBM segmentation and diffusion-based tracking of NBM white matter projections, and computed white matter hypointensities (WM-hypo) as a marker of SVD. We successfully tracked pathways that closely resemble the spatial layout of the cholinergic system as seen in previous post-mortem and DTI tractography studies. We found that high WM-hypo load was associated with older age, male sex, and lower performance in attention and memory. A high WM-hypo load was also associated with lower integrity of the cholinergic system above and beyond the effect of age. In a multivariate model, age and integrity of NBM white matter projections were stronger contributors than WM-hypo load and NBM volume to performance in attention and memory. We conclude that the integrity of NBM white matter projections plays a fundamental role in cognitive aging. This and other modern neuroimaging methods offer new opportunities to re-evaluate the cholinergic hypothesis of cognitive aging.

1. Introduction

Cholinergic neurons in the central nervous system provide vital control over brain circuitry responsible for cognitive functions such as memory and attention. Since its discovery, the cholinergic circuitry of the basal forebrain (BF) has been scrutinized for its possible involvement in cognitive decline characteristic of aging and age-related disorders including Alzheimer's disease (AD) and vascular cognitive impairment (Bartus et al., 1982; Drachman and Leavitt, 1974). Most of the cholinergic neurons are located in the BF nuclei (Ch1-4), as well as in the

* Corresponding author. Division of Clinical Geriatrics, Center for Alzheimer Research, Department of Neurobiology, Care Sciences and Society, NEO floor 7th, Karolinska Institutet, 141 57, Huddinge, Stockholm, Sweden.
E-mail address: daniel.ferreira.padilla@ki.se (D. Ferreira).

https://doi.org/10.1016/j.neuroimage.2020.116607
Received 25 November 2019; Received in revised form 23 January 2020; Accepted 3 February 2020
Available online 6 February 2020

pedunculo-pontine and laterodorsal tegmental nuclei in the brainstem (Ch5-6). All these regions serve together as the major sources of cholinergic projection neurons to the entire neocortex, amygdala, thalamus, and hippocampus (Mesulam et al., 1983; Woolf, 1991). However, it is the cholinergic neurons located in the nucleus basalis of Meynert (NBM, Ch4) that provide the major cholinergic input to cortical areas, and have stronger involvement in cognition.

The identification of the cholinergic cell bodies that innervate the cerebral cortex was made possible by visualization of the hydrolytic enzyme acetylcholinesterase (AChE) (Mesulam and Van Hoesen, 1976) and by immunolabeling with the synthetic enzyme of acetylcholine, choline acetyltransferase (ChAT) (Mesulam et al., 1986). More recently, magnetic resonance imaging (MRI) has been used to investigate the characteristics of the cholinergic BF *in vivo* using automated volumetric measurements of the BF structure. *In vivo* measurement of the BF has been facilitated through the development of stereotactic mappings of the cholinergic BF nuclei in MRI standard space based on cytoarchitectonic maps derived from combined histology and *post-mortem* MRI of autopsy brains (Kilimann et al., 2014; Teipel et al., 2005; Zaborszky et al., 2008). Using these cytoarchitectonic mappings as BF region of interest (ROI), a number of volumetric *in vivo* studies have shown BF atrophy in advanced aging (Grothe et al., 2013, 2012), AD dementia (Teipel et al., 2011, 2005), and mild cognitive impairment (MCI) (Grothe et al., 2010; Teipel et al., 2014). These studies could also demonstrate robust associations of BF atrophy with cognitive deficits in neurodegenerative diseases (Grothe et al., 2010, 2016), but findings on the relationship between BF structure and cognitive performance in normal aging remain inconclusive (Butler et al., 2012; Lammers et al., 2018, 2016; Wolf et al., 2014).

The cholinergic white matter (WM) projections from the NBM to the entire brain have been less widely investigated. A seminal *post mortem* study using AChE and ChAT cholinergic markers in whole-hemisphere sections identified two major cholinergic pathways, i.e. medial and lateral, passing from the NBM to the cortex (Selden et al., 1998). The medial pathway joins the WM of the gyrus rectus, curves around the rostrum to the corpus callosum, and enters the cingulum bundle, supplying the parolfactory, cingulate, and retrosplenial cortices. The lateral pathway has a perisylvian division which supplies the frontoparietal operculum, insula, and superior temporal gyrus, and a capsular division traveling in the external capsule and uncinate fasciculus, supplying the remaining parts of the frontal, parietal, and temporal neocortex. However, the precise topography of the NBM cholinergic projections to the cerebral cortex is yet unknown. MRI techniques based on resting-state functional MRI (rs-fMRI) and diffusion tensor imaging (DTI) could provide further information on the NBM cholinergic pathways *in vivo*. The rs-fMRI technique measures the spontaneous blood oxygenation level-dependent (BOLD) signal in the absence of any explicit task. This technique was recently used to investigate coordinated signal fluctuations between the BF and the cortex, revealing distinct functional connectivity patterns of the BF (Fritz et al., 2019). DTI is commonly used to assess WM microstructural integrity. Previous voxel-based DTI studies showed an association between reduced NBM volume and reduced integrity across widespread WM areas, possibly involving NBM cholinergic tracts as well (Teipel et al., 2014, 2011). Unlike voxel-based DTI analysis, probabilistic tracking can in principle reveal WM pathways connected to specific regions such as the NBM, thus providing information on cholinergic NBM WM projections in a probabilistic manner.

So far only one study used DTI to track the NBM cholinergic pathways. This study included a cohort of 25 patients with vascular cognitive impairment and 24 healthy controls (Liu et al., 2017), and showed that vascular cognitive impairment was associated with reduced integrity of NBM pathways, but not with NBM volume per se. WM hyperintensities on T2/FLAIR sequences, which appear as WM hypointensities on T1-weighted images (Wardlaw et al., 2013), are the main MRI finding associated with vascular cognitive impairment. Interestingly, WM hyperintensities are also commonly found in cognitively normal individuals (Gunning-Dixon et al., 2009), and are related to lower cognitive performance and subjective cognitive complaints in these individuals (Cedres et al., 2019; Hawkins et al., 2017; Nunley et al., 2015). These and other findings highlight the role of cerebral small vessel disease (SVD) in cognitive aging (Yang et al., 2017). Of interest, several lines of evidence suggest a central role of cholinergic deficiency in vascular cognitive impairment (Liu et al., 2017). However, the connection between SVD and cholinergic dysfunction to explain age-related cognitive decline is still unclear. The cholinergic hypothesis of cognitive aging postulates that functional disturbances in cholinergic activity occur in the brains of healthy older adults, contributing to their characteristic memory decline and related cognitive problems (Bartus et al., 1982; Dumas and Newhouse, 2011). Hence, we aimed to investigate the contribution of SVD and the integrity of the cholinergic system towards cognitive performance in cognitively normal middle-aged and older individuals. Our first aim was to identify NBM WM projections by using DTI tractography in a large cohort of cognitively normal individuals (N = 262, 39–77 years of age). We report constrained DTI tractography models guided by the findings of the only previous study in the field (Liu et al., 2017). In addition, we report unconstrained models to examine other potential cholinergic projections in an exploratory manner. Our second aim was to investigate the association of SVD (WM hypointensities) with the integrity of the cholinergic system and cognitive functions known to be mediated by the cholinergic circuitry, specifically, attention and memory (Ballinger et al., 2016). Because the effect of aging is central in this study, we report our findings in a stepwise manner: without any correction, with a correction for the effect of sex and crystallised intelligence, and with a correction for the effect of age on top of the previous correction. This strategy enables an easy and direct understanding of the role of the age variable in all our models. In addition, we also modelled the effect of age in multivariate models.

2. Materials and methods

2.1. Participants

A total of 262 individuals (39–77 years of age) were selected from the GENIC-database (Ferreira et al., 2014; Machado et al., 2018), a community-based cohort from the Canary Islands (Spain). Inclusion criteria for the current study were: (1) Normal cognitive performance in comprehensive neuropsychological assessment using pertinent clinical normative data and excluding individuals with performance below 2 SD using own sample descriptive values (i.e., individuals did not fulfil cognitive criteria for MCI or dementia); (2) preserved activities of daily living and global cognition operationalized as a Functional Activity Questionnaire (FAQ) (Pfeffer et al., 1982) score $\leq$ 5, a Blessed Dementia Rating Scale (BDRS) (Blessed et al., 1968) score $\leq$ 4, and a Mini-Mental State Examination (MMSE) (Folstein et al., 1975) score $\geq$ 24 (the MMSE cut-point of $\geq$24 is used for screening according to the demographic characteristics of our cohort, but cognitive impairment is ruled out using comprehensive neuropsychological assessment as described in criterion #1 above); (3) Availability of MRI data; (4) No abnormal findings such as stroke, tumors, hippocampal sclerosis, etc., in MRI according to an experienced neuroradiologist; (5) no medical history of neurological or psychiatric disorders (including a diagnosis of major depression), systemic diseases or head trauma; and (6) no history of substance abuse. Subjects' recruitment in the GENIC-database was done through primary care health centers, advertisements in local schools, and relatives and acquaintances of the research staff, covering a representative sample in terms of age, sex, and education. Participation was completely voluntary and all the participants gave written informed consent approved by the local ethics committee.

2.2. Clinical and cognitive assessment

From an extensive neuropsychological protocol fully described elsewhere (Ferreira et al., 2015), the following tests of memory and attention

were selected according to the aims of the current study: TAVEC (Benedet MJ, 1998), the Spanish version of the California Verbal Learning Test (CVLT), was used to measure verbal episodic memory. We included the total learning score after 5 learning trials, delayed recall after 5 min, delayed recall after 30 min, and recognition (higher values reflect better performance). Attention was measured with the first sheet (words) of the Stroop test (Stroop, 1935), as well as the Choice Reaction Times task of the PC-Vienna System (PCV – reaction time) (Schuhfried, 1992). The Stroop test – first sheet is a verbal task with higher demands on focussed attention, whereas the Choice Reaction Times is a visual task with higher demands on vigilance. For the Stroop test, participants were given 45 s to complete the task and the score obtained was the total number of words correctly read (higher values reflect better performance). For Choice Reaction Times, participants underwent a 15-min computerised vigilance task in which a response is required when a specific stimulus is displayed. Time is recorded, with higher time values and errors denoting worse performance. Both Stroop and PCV are also common tests for processing speed. Stroop is also a traditional measure for executive functioning, and PCV includes a component of motor inhibition. Depressive symptomatology was assessed with the Beck Depression Inventory (BDI, 21-item version) (Beck et al., 1961) in individuals younger than 63 years of age, and the Geriatric Depression Scale (GDS, 15-item version) (Yesavage and Sheikh, 1986) in individuals 63 years old or older. The original scores from both scales were z-transformed and combined into a single measure (BDI-GDS composite), as in previous studies (Machado et al., 2018). The Information subtest from the Wechsler Adult Intelligence Scale – Third Revision (WAIS-III) (Wechsler, 1997) was scored and used as an indicator of crystallised intelligence. In addition, global cognition was assessed with the MMSE (Folstein et al., 1975), and activities of daily living with the FAQ and the BDRS (Blessed et al., 1968).

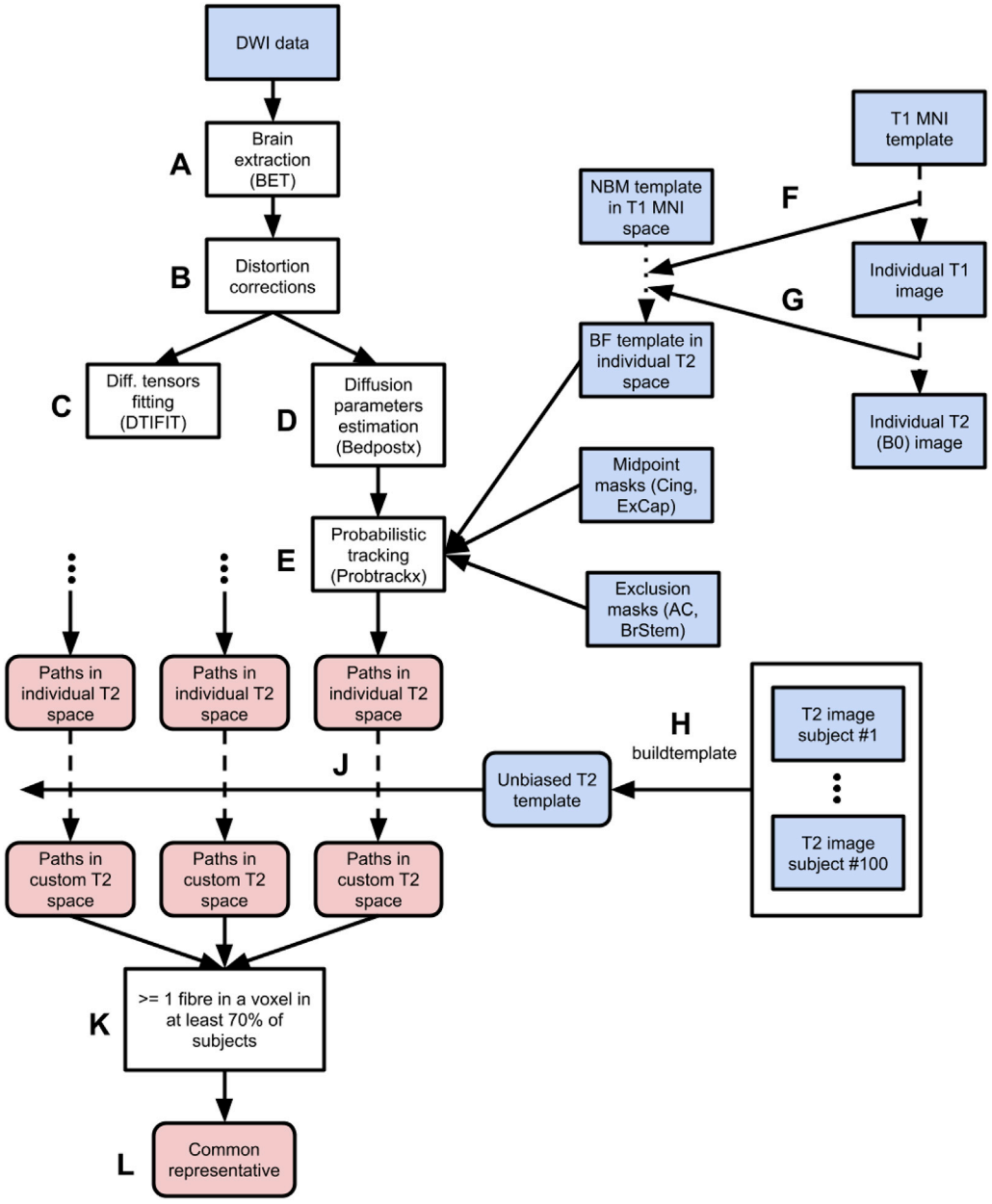

Fig. 1. Study pipeline. White boxes, programs and processes; Blue boxes, T1 and T2 images; Red boxes, tracts. DWI, diffusion-weighted imaging; NBM, nucleus basalis of Meynert; MNI, Montreal Neurological Institute; AC, anterior commissure; BrStem, brain stem. T2 images are B0 images (DWI b = 0). The I letter was intentionally omitted to improve readability.

2.3. MRI acquisition

Participants were scanned using a 3.0 T GE imaging system (General Electric, Milwaukee, WI, USA) located at the *Hospital Universitario de Canarias* in Tenerife, Spain. A three-dimensional T1-weighted fast spoiled gradient echo (FSPGR) sequence was acquired in the sagittal plane with the following parameters: repetition time/echo time = 8.73/1.74 ms, inversion time = 650 ms, field of view 250 × 250 mm, matrix 250 × 250 mm, flip angle 12°, slice thickness = 1 mm. A DTI sequence was acquired in the axial plane. The parameters were as follows: repetition time/echo time = 15000/≈72 ms, field of view 256 × 256 mm, matrix 128 × 128 mm, flip angle 90°, slice thickness = 2.4 mm, 31 isotropically distributed gradient orientations (b = 1000 s/mm^2), and 1 image without diffusion weighting (b = 0 s/mm^2, b0). Full brain and skull coverage was required for the MRI datasets and detailed quality control was carried out on all MR images according to previously published criteria (Simmons et al., 2009).

The whole processing pipeline for the MRI data is shown in Fig. 1 and is explained in detail in the next sections.

2.4. MRI data pre-processing

The DTI data were processed using the FSL toolbox (version 5.0.9, FMRIB, Oxford, UK) (Jenkinson et al., 2012). First, the non-brain tissues were removed using FSL's automated brain extraction tool (Jenkinson et al., 2005) (BET, Fig. 1A) and corrected for eddy currents and head motion (Andersson and Sotiropoulos, 2016) (Fig. 1B), followed by fitting of diffusion tensors (Fig. 1C). Next, the algorithm implemented in FSL (BedpostX) was used to calculate the diffusion parameters in a standard ball-and-sticks model (Behrens et al., 2007) for each voxel (Fig. 1D), considering 3 fibres modelled per voxel.

2.5. ROI masks and tractography

Six ROI masks were used in this study: an ROI mask of the NBM was used as the initiating seed region for probabilistic tracking; cingulum and external capsule ROI masks as midway regions for the constrained tractography model (see next paragraph); ROI masks of the anterior commissure and brainstem were used as exclusion masks in both constrained and unconstrained models (see next paragraph); and finally, an ROI of remaining WM (please see below) as a negative control mask. The NBM ROI was based on a cytoarchitectonic map of BF cholinergic nuclei in MNI space, derived from combined histology and *in cranio* MRI of a *post-mortem* brain (Kilimann et al., 2014). We obtained the NBM ROI by combining the anterior lateral, intermediate, and posterior regions of the Ch4 region of the BF mask (Kilimann et al., 2014). The cingulum and external capsule masks were based on the Johns Hopkins University (JHU) WM atlas, available as part of the FSL package (Mori et al., 2005). The cingulum and external capsule masks were also used in the previous study by Liu et al. (2017), to constrain the NBM WM tracts. The brainstem ROI mask was extracted using FSL's FIRST segmentation routine (Patenaude et al., 2011). The anterior commissure ROI mask was delineated in the MNI template by a trained expert (O.L.). The remaining WM mask was created by excluding the cholinergic tracts described below (i.e. union of external capsule and cingulum pathways) from the whole WM mask. The whole WM mask was obtained from the FSL's Automated Segmentation Tool (FAST) (Zhang et al., 2001). These six ROI masks were registered into each subject's individual space. For this purpose, the registration parameters from individual T1 space to standard T1 MNI space were inversely applied to the NBM, anterior commissure, and brainstem masks (Fig. 1F), following registration to native diffusion space (Fig. 1G). For the cingulum and external capsule ROI masks defined in a standard space DTI template, the registration parameters of an individual DTI image (B0 image) to the standard DTI template were inversely applied to register the masks from standard space to native space. All registration steps (T1 -> T1-MNI and DTI -> DTI-MNI) were carried out using the non-linear SyN registration algorithm (Avants et al., 2008) in Advanced Normalization Tools (ANTs, http://stnava.github.io/ANTs/).

Probabilistic tracking was performed by repeating 5000 random samples from each of the NBM ROI voxels and propagated through the local probability density functions of the estimated diffusion parameters (Fig. 1E). This procedure was performed in two manners: (1) a constrained manner, in which only those streamlines initiated from the NBM ROI that reach a voxel in midway cingulum or external capsule ROI masks were retained. The aim of conducting these models was to reconstruct the two major NBM cholinergic pathways projecting through the cingulum and the external capsule (Liu et al., 2017; Selden et al., 1998); (2) an unconstrained explorative manner, with streamlines initiating in the NBM and propagating across the brain with no midway constrains other than the exclusion anterior commissure and brainstem ROI masks, to avoid contamination from non-cholinergic pathways going through the anterior commissure as well as connecting to the cerebellum and medulla. The brainstem contribution to cortical cholinergic innervation is small (Mesulam, 2013). The aim of conducting this unconstrained model was to explore potential cholinergic projections not covered by the constrained model. The anterior commissure and brainstem exclusion masks were also used for the constrained models.

2.6. Common pathways

Individually tracked pathways were brought to a common space to be able to compare them across individuals. For this purpose, an unbiased template was created from 100 randomly selected pre-processed B0 images using the *buildtemplate* module in ANTs (Fig. 1H). Briefly, the initial template was obtained by taking the average of all 100 image volumes. Each image volume was then co-registered to the initial template and the average was calculated again to obtain a refined template. This process continued for 4 iterations using the non-linear registration algorithm SyN (Avants et al., 2008). The template obtained is referred to as the unbiased template. Next, warping fields co-aligning individual input B0 images to the unbiased template were used to translate the individual tracking results to the same anatomical space (Fig. 1J).

We derived a *common representative* for each tract, similar to that done in previous studies (de Reus and van den Heuvel, 2013; Liu et al., 2017). This procedure consists in thresholding all individual tracts (in the space of the unbiased template) so that only those voxels that were met by at least one tracked fibre (i.e. threshold $\geq$1) were counted (de Reus and van den Heuvel, 2013). Then, all these thresholded individual images were considered and only the voxels that were present in at least 70% of the (thresholded) cases (Fig. 1K) were retained in the final binary mask of the common representative tract (Liu et al., 2017) (Fig. 1L). The group threshold was chosen by visual inspection so that the resulting pathways were extensive, yet still specific. In contrast to (Liu et al., 2017), we did not restrict the final masks to skeletonized pathways because our aim was to identify NBM WM projections beyond and above the WM skeleton; and we used a non-linear registration tool due to the small size of the NBM. The methodological differences with de Reus and van den Heuvel (2013) are that we investigated cholinergic pathways based on probabilistic tractography, whereas de Reus and van den Heuvel (2013) used whole-brain networks based on deterministic tractography.

2.7. Extraction of diffusivity indices

To characterize the microstructure properties of the tracked cholinergic pathways, we extracted the mean diffusivity (MD) index. The MD index is sensitive to conditions that affect the barriers that restrict the movement of water, such as cell membranes (Zhang et al., 2014). We selected the MD index because it has been shown to precede changes in other DTI indexes (e.g. fractional anisotropy), as well as in the gray matter volume in pre-symptomatic individuals with familial AD (Li et al., 2015), preclinical individuals with sporadic AD (Li et al., 2014), and

individuals with AD (Acosta-Cabronero et al., 2010). Also, increased MD in the cingulum and inferior fronto-occipital fasciculus was associated with lower performance in several visual abilities of the posterior cortex in cognitively normal middle-aged individuals from the same cohort as used in the current study (Ferreira et al., 2017). Further, MD is less susceptible than fractional anisotropy to alterations due to different fibre populations in individual voxels (i.e. the crossing fibres problem). For the sake of simplicity, all representative tracts were back-transformed into individual DTI space for each subject and single number summaries were computed - an average value of MD along each representative tract. The same procedure was applied to the negative control remaining WM mask.

2.8. NBM volume

Individual NBM volumes were calculated by summing up the number of gray matter (GM) voxels within the back-transformed NBM ROI in each individual's native T1-weighted space. GM segmentation was obtained from the FSL's Automated Segmentation Tool (Zhang et al., 2001) (FAST). The total intracranial volume (TIV) was estimated based on the affine transform in the FreeSurfer 5.1.0 image analysis suite (http://surfer.nmr.mgh.harvard.edu/). NBM volumes were divided by the TIV in order to account for between-subjects variability in head size (Buckner et al., 2004).

2.9. WM hypointensities (WM-hypo)

We used WM hypointensities (WM-hypo) as a marker of SVD (Wardlaw et al., 2013). WM-hypo on T1-weighted images appear as WM hyperintensities on T2/FLAIR sequences (Wardlaw et al., 2013), and correlate with microstructural WM changes as measured on diffusion tensor imaging data (Leritz et al., 2014). Further, there is a strong correlation between WM-hypo and WM hyperintensities (Cedres et al., 2020). Segmentation of WM-hypo and corresponding volumetrics was performed on T1-weighted images using the probabilistic procedure implemented in FreeSurfer 5.1.0, subsequently extended to label WM lesions (Brands et al., 2006; Fischl et al., 2002). This procedure has demonstrated good sensitivity in measuring WM damage both in healthy individuals and in AD patients (Leritz et al., 2014; Salat et al., 2010).

2.10. Statistical analysis

Statistical analysis was carried out using the R programming language (The R Foundation for Statistical Computing; version 3.5.1). Results were deemed statistically significant at two-tailed $p < 0.05$.

Because our aim was to investigate the role of SVD, we used Gaussian mixture model estimated by expectation-maximization algorithm to identify two groups with respect to the WM-hypo load (high WM-hypo and low WM-hypo load) (Fig. 2). Demographics were compared between the high and low WM-hypo load groups using independent *t*-tests for age and Chi-square tests for sex. All cognitive measures were compared between groups in a one-way analysis of variance with covariates (ANCOVA), controlling for age, sex, and WAIS-III Information. For a better understanding of the role of these variables in our findings, in particular the role of the age variable, we report the outcome of these analyses in a stepwise manner: without any correction, with a correction for the effect of sex and WAIS-III Information as a measure of crystallised intelligence, and with a correction for the effect of age on top of the previous correction. The extracted NBM volume corrected for the TIV was also compared using ANCOVA, controlling for age, sex, and WAIS-III Information (stepwise manner). To assess whether SVD influences tract integrity, ANCOVA was applied to test for differences between high and low WM-hypo load groups in tract-specific MD measures, controlling for age, sex, and WAIS-III Information (stepwise manner). The degree of contribution of age, sex, WAIS-III Information, MD in the cingulum, external capsule tracts and in the remaining WM, NBM volume, WM-hypo, and MMSE scores to domain-specific cognitive measures was

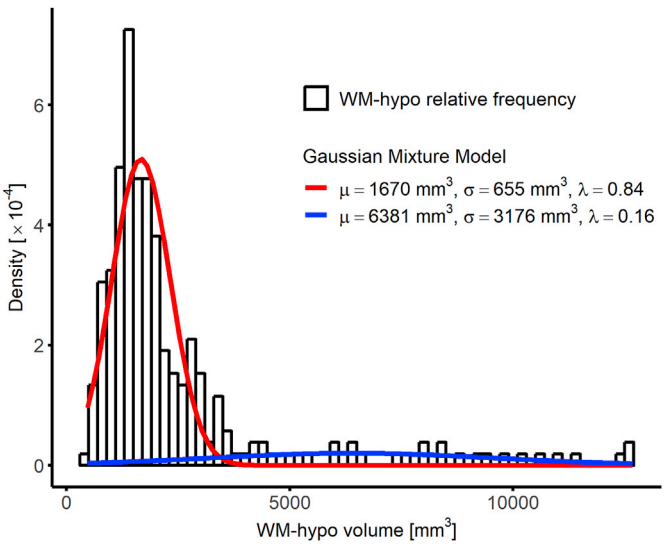

Fig. 2. Gaussian mixture model fit to separate the cohort into two groups of high and low WM-hypo load. Mixture components are characterized by Gaussian distribution with a mean value μ and a standard deviation σ; λ is a mixture weight. The intersection of the two scaled probability distribution functions (WM-hypo = 3400 mm^3) defines the threshold between the low and high WM-hypo load groups. WM-hypo, WM hypointensities on T1-weighted images appearing as WM hyperintensities on T2/FLAIR sequences (Wardlaw et al., 2013).

investigated with random forest analysis. We used random forest regression (with conditional inference tree for unbiased variable selection) instead of multiple linear regression/mediation analyses because we wanted to investigate the interactive contribution of the predictors, rather than partial effects (Machado et al., 2018). Random forest (RF) is an ensemble method in machine learning that involves growing of multiple decision trees via bootstrap aggregation (bagging). Each tree predicts a classification independently and votes for the corresponding class. The majority of the votes decides the overall prediction (Breiman, 2001, 1996). Conditional feature importance scores for random forest were computed by measuring the increase in prediction error if the values of a variable under question are permuted within a grid defined by the covariates that are associated to the variable of interest. This score is computed for each constituent tree, averaged across the entire ensemble. The conditional feature importance scores were designed to diminish an undesirable effect of preference of correlated predictor variables. The random forest was comprised of 2000 conditional inference trees. The *party* package (Strobl et al., 2007) was used in this analysis. For the sake of completeness, we also report Pearson correlation coefficients among the variables included in the random forest analysis (the point-biserial correlation coefficient was computed for the dummy variable of sex).

2.11. Data and code availability

Requests for access to the data and code used in this study should be directed to the corresponding author. Our data sharing complies with the requirements of our funders and institutes, as well as with institutional ethics approval.

3. Results

3.1. Association between WM-hypo, demographic variables and cognitive performance

Demographic data are shown in Table 1. The high WM-hypo load group was significantly older, included a higher frequency of men, had higher values in the BDRS score, and showed worse cognitive

Table 1

Demographic and clinical variables by WM-hypo load groups [mean value (SD), or count]. For age, an independent *t*-test was performed ($df = 48$; equal variances not assumed). For sex, a chi-square test was performed. For all other variables, one-way ANCOVA were performed by setting the group (low/high WM-hypo load) as the independent variable and WAIS-III Information, age, and sex as covariates ($df = 1, 260$). Since depressive symptomatology was measured with BDI or GDS, original scores were Z-transformed in order to combine both measures (BDI-GDS composite). *$p < 0.05$, **$p < 0.01$, ***$p < 0.001$ (assessed using a two-tailed alpha). M, male; F, female; WAIS-III, Wechsler Adult Intelligence Scale – Third revision; BDRS, Blessed Dementia Rating Scale; FAQ, Functional Activity Questionnaire; GDS, Geriatric Depression Scale; BDI, Beck Depression Inventory; MMSE, Mini-Mental State Examination; PCV – reaction time, PC-Vienna cognitive reactive time; TAVEC, the Spanish version of the California Verbal Learning Test (CVLT) (TAVEC: *Test de Aprendizaje Verbal España-Complutense*); NBM volume, volume of nucleus basalis of Meynert; TIV, total intracranial volume; WM-hypo, WM hypointensities on T1-weighted images appearing as WM hyperintensities on T2/FLAIR sequences (Wardlaw et al., 2013).

	Entire cohort	Low WM-hypo load group	High WM-hypo load group	$t/\chi^2/F_{1,260}$ (no correction)	$F_{1,258}$ (corrected for sex and WAIS-III Information)	$F_{1,257}$ (corrected for sex, WAIS-III Information, and age)
Count, n	262	226	36			
Age	55.6 (10.4)	53.9 (9.54)	65.2 (8.9)	−7.1***		
Sex (M/F)	122/140	97/129	25/11	8.8**		
WAIS-III Information	16.6 (5.9)	16.6 (5.9)	16.5 (5.9)	0.1		
BDRS	0.9 (1.5)	0.8 (1.3)	1.4 (2.15)	4.3*	3.6	1.6
FAQ	0.4 (0.8)	0.4 (0.8)	0.4 (0.6)	0.1	0.4	0.4
BDI-GDS composite	0 (1)	−0.04 (0.92)	0.15 (1.32)	1.2	1.6	1.3
MMSE	28.8 (1.3)	28.8 (1.2)	28.5 (1.4)	2.0	0.5	0.3
PCV – reaction time	476 (82.1)	471.0 (74.8)	511.0 (111.0)	7.9**	7.2**	0.0
STROOP – words	99.5 (18.9)	99.9 (18.6)	97.5 (21.2)	0.5	0.3	1.4
TAVEC learning	55.3 (9.1)	56.0 (9.2)	51.8 (7.4)	6.7*	2.8	0.2
TAVEC delayed recall (5 min)	11.6 (2.8)	11.8 (2.7)	10.4 (2.6)	8.8**	4.6*	0.1
TAVEC delayed recall (30 min)	13.6 (2.5)	13.8 (2.5)	12.7 (2.3)	6.8**	3.4	0.1
TAVEC recognition	15.6 (0.6)	15.7 (0.6)	15.4 (0.9)	4.5*	2.9	1.1
NBM volume (TIV corrected)	0.00025 (0.00003)	0.00025 (0.00003)	0.00023 (0.00004)	9.10**	7.87**	8.47**

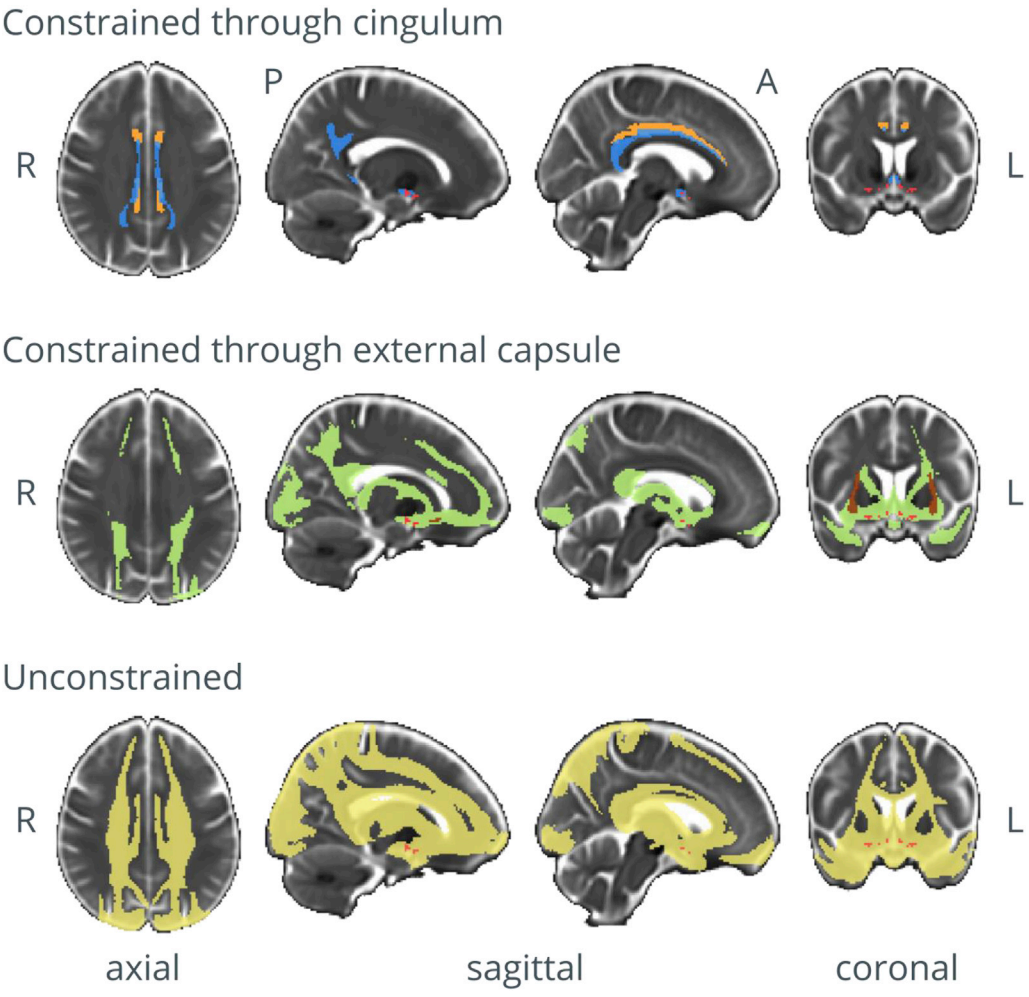

Fig. 3. Cholinergic WM pathways. Red for NBM ROI mask. (First row) Orange for the cingulum mask, blue for the pathway passing through the cingulum. (Second row) Brown for the external capsule mask, green for the pathway passing through the external capsule. (Third row) Yellow for the pathway without restrictions (no explicit midpoint masks). Tracks passing through voxels in anterior commissure and brainstem regions were excluded in the three models using the pertinent masks (please see Methods section). R, right; L, left; A, anterior; P, posterior.

performance in PCV – reaction time and all TAVEC memory measures. When controlling for sex and the WAIS-III Information subtest as a measure of crystallised intelligence, the WM-hypo groups significantly differed in PCV - reaction time and TAVEC delayed recall (5 min). These differences were no longer significant when adding age as a covariate on top of sex and WAIS-III Information (please see the stepwise analysis in Table 1).

3.2. Association between WM-hypo and NBM volume

The NBM volume (corrected for the total intracranial volume, TIV) was significantly smaller in the high WM-hypo load group (Table 1), both without and with controlling for sex, WAIS-III Information, and age.

3.3. Cholinergic pathways

Fig. 3 shows the tracked cholinergic pathways in the probabilistic analyses. The constrained models showed that the medial pathway (in blue) projects from the NBM through gyrus rectus to cingulum and continues to cingulate cortex and retrosplenial cortex. For the lateral pathway (in green), the external capsule division was successfully tracked to inferior frontal cortex (frontal pole) through the uncinate fasciculus, as well as to parietal and temporal cortex via posterior thalamic radiation and internal capsule. Even though no explicit guidance (midway mask) was used for the perisylvian division of the lateral pathway, this division was also successfully tracked throughout the insula, superior temporal gyrus, and frontoparietal operculum. The unconstrained model (in yellow) included the areas described for the medial and lateral pathways but was more widespread including other brain areas such as the posterior cingulate and superior medial areas of parietal and frontal lobes. However, the unconstrained model also included voxels from the posterior regions of the lateral ventricles.

3.4. Association between WM-hypo and integrity of the cholinergic pathways

The high WM-hypo load group showed significantly higher mean diffusivity (MD) values in the tracked cingulum and external capsule pathways as compared with the low WM-hypo load group, after controlling for sex, WAIS-III Information, and age (Table 2). In contrast, WM-hypo load did not have any significant effect on the negative control remaining WM, after controlling for sex, WAIS-III Information, and age (Table 2).

3.5. The contribution of age, WM-hypo, and integrity of the cholinergic system towards cognitive performance

The distinct contributions of MD in the cingulum and external capsule pathways, MD in remaining WM, WM-hypo (as a continuous variable), and NBM volume towards cognitive measures were examined by a random forest analysis, also including age, sex, WAIS-III Information, and the MMSE score as predictors in the models. The unconstrained model was not considered for these analyses because we were interested in specific pathway-cognition associations, and the unconstrained model is reported only for consideration of potential false negatives in the constrained models.

Overall, MD in the external capsule pathway had a stronger importance in the prediction of TAVEC delayed recall (both 5 min and 30 min; Fig. 4). MD in the cingulum pathway had a stronger importance in the prediction of PCV – reaction and TAVEC delayed recall (30 min). Performance in Stroop and TAVEC learning was mainly predicted by WAIS-III Information. MMSE, sex, and age were also important for the prediction of TAVEC learning. Although the age contributed to the prediction of performance in all our cognitive tasks, its contribution was lower than MD in the cholinergic pathways in TAVEC delayed recall (both 5 min and 30 min). WM-hypo, NBM volume, and remaining WM received low importance scores in all the random forest models. The random forest model for TAVEC recognition did not perform better than random prediction.

Fig. 5 shows the correlation matrix for all pairs of predictors of the random forest models. Age, WM-hypo, and MD in the cholinergic pathways were highly correlated with each other.

4. Discussion

In this study, we investigated the contribution of SVD and the integrity of the cholinergic system to attention and memory in normal aging. We found that high WM-hypo load, a marker of SVD, was associated with older age and male sex. High WM-hypo load was also associated with lower performance in attention and memory, but this effect was largely explained by age. In contrast, high WM-hypo load was associated with lower integrity of the cholinergic system (both NBM volume and NBM WM projections) above and beyond the effect of age. The multivariate models showed that reduced integrity of the cholinergic pathways and age, but not WM-hypo load or NBM volume, strongly contributed to performance in attention and memory in our cohort of cognitively normal middle-aged to older individuals.

We found that the WM-hypo load was higher in older individuals and in males. The same finding has repeatedly been reported in previous studies (Habes et al., 2016; Raz et al., 2012). We also found that lower performance in attention and memory in the high WM-hypo load group was accounted for by older age (and to some extent also by male sex and WAIS-III Information). This result is in line with a previous study (Gustavsson et al., 2015). Whether WM-hypo in cognitively normal older individuals indicate preclinical stages of vascular cognitive impairment or are rather a feature of normal aging when not reaching the clinical threshold is currently not known. Our data show a strong association between WM-hypo and age. However, WM-hypo do not seem to have a direct impact on attention or memory but rather an indirect effect through age and integrity of the cholinergic pathways (discussed further down).

An important finding of the current study is that, in contrast to the results on attention and memory, higher WM-hypo load was associated with lower NBM volume and reduced integrity of the cholinergic pathways above and beyond the effect of age. A previous study showed no significant association between NBM volume and vascular cognitive impairment (Liu et al., 2017). A possible explanation for the discrepancy could be the smaller sample size in the study by Liu et al. (2017). This

Table 2
Association between WM-hypo and mean diffusivity in the cholinergic NBM pathways [mean value (SD)] in high and low WM-hypo load groups. MD, mean diffusivity; WM-hypo, WM hypointensities on T1-weighted images appearing as WM hyperintensities on T2/FLAIR sequences (Wardlaw et al., 2013). *$p < 0.05$, **$p < 0.01$, ***$p < 0.001$.

	Low WM-hypo load group	High WM-hypo load group	$F_{1,260}$ (no correction)	$F_{1,258}$ (corrected for sex and WAIS-III Information	$F_{1,257}$ (corrected for sex, WAIS-III Information, and age)
MD in cingulum pathway	0.00083 (0.00003)	0.00089 (0.00006)	72.1***	62.6***	23.2***
MD in external capsule pathway	0.00090 (0.00005)	0.00102 (0.00009)	141.7***	127.3***	69.0***
MD in remaining WM	0.00079 (0.00003)	0.00080 (0.00003)	5.9*	6.6*	0.5

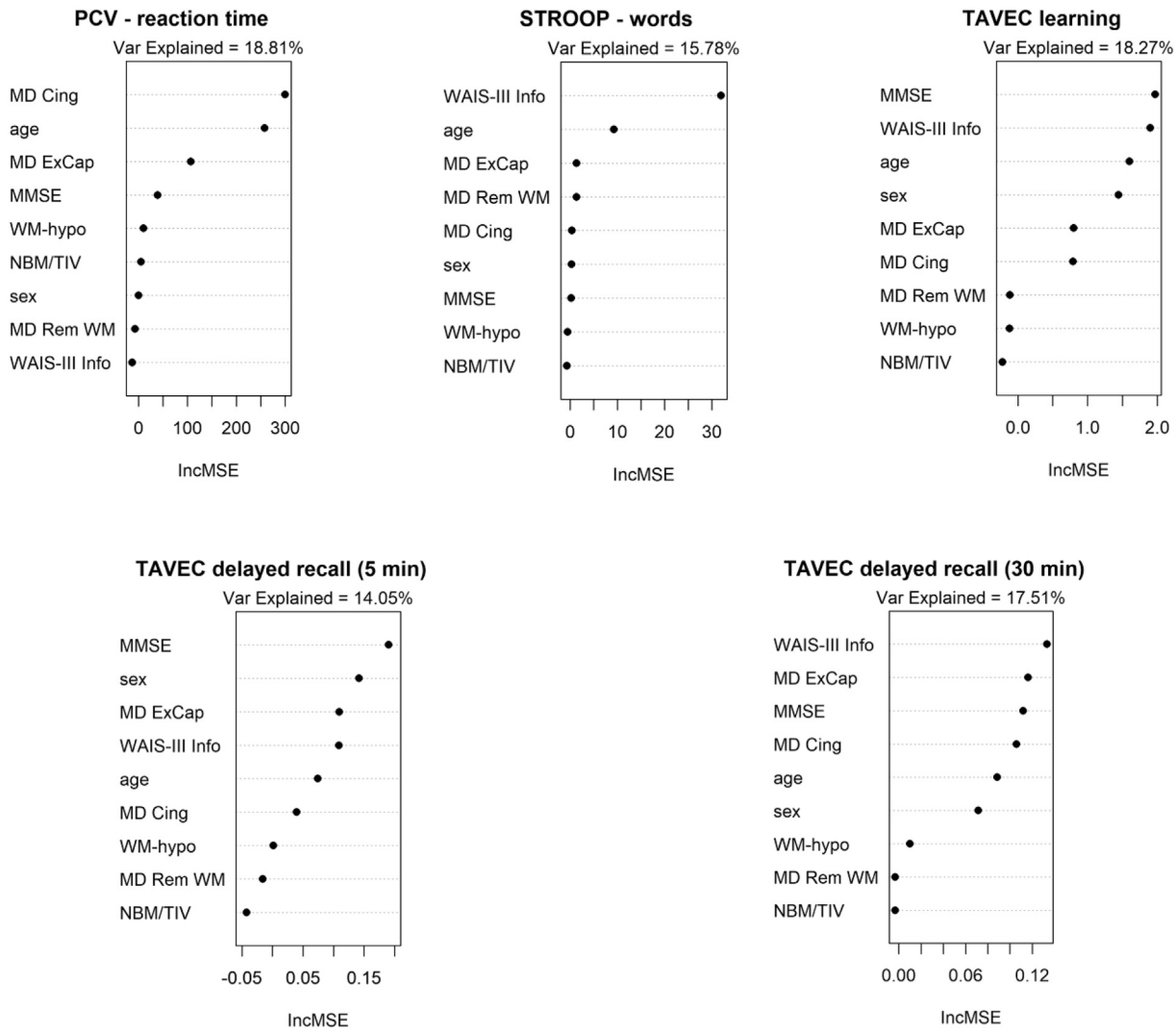

Fig. 4. Random forest models (increase in prediction error). MMSE, Mini-Mental State Examination; MD, mean diffusivity; ExCap, external capsule tract; Cing, cingulum tract; Rem WM, WM excluding cholinergic tracts; WAIS-III Info, Wechsler Adult Intelligence Scale – Third revision Information subtest; WM-hypo, WM hypointensities on T1-weighted images appearing as WM hyperintensities on T2/FLAIR sequences (Wardlaw et al., 2013); NBM/TIV, volume of nucleus basalis of Meynert scaled by total intracranial volume. IncMSE, conditional variable importance computed by increase in the mean square error of prediction as a result of a corresponding variable being permuted within a grid defined by the covariates that are associated to the variable of interest.

could potentially make it difficult to capture an association between SVD and NBM volume. Another possible explanation relates to methodological differences; SVD, one of the criteria for defining vascular cognitive impairment in Liu et al. (2017), was assessed by the Fazekas rating scale, which gives 4 rough scores from 0 to 3 based on 2D images across a limited set of brain sections. In contrast, we assessed SVD with an automated estimation of WM-hypo volume in 3D images across the entire WM. Furthermore, it is also possible that the association between NBM degeneration and SVD is stronger in normal aging, while this association may be weaker or non-existent in patients with a diagnosis of vascular cognitive impairment.

Probabilistic tractography analysis to track white matter pathways arising from the NBM was conducted in order to evaluate the integrity of these tracts *in vivo*. Our constrained models successfully revealed tracts in both medial and lateral pathways, as previously shown using AChE histochemical and ChAT and NGFr immunohistochemical analysis (Selden et al., 1998), as well as in the previous DTI tractography study (Liu et al., 2017). Our unconstrained model included the areas covered by the medial and lateral pathways and extended to other brain areas such as the posterior cingulate and superior medial areas of parietal and frontal lobes. Large portions of these areas have also been labelled as cholinergic projections in histochemical and immunohistochemical studies (Selden et al., 1998), and underlie cortical areas depicted in a recent rs-fMRI study (Fritz et al., 2019). This information may be relevant when it comes to considering potential false negatives in the cingulum and external capsule models. However, we acknowledge that the unconstrained model also included voxels from the lateral ventricles.

We found that high WM-hypo load was associated with reduced integrity in the two cholinergic pathways and the unconstrained model above and beyond the effect of age. Liu et al. (2017) also found that vascular cognitive impairment was associated with reduced integrity in medial and lateral cholinergic pathways. Thus, WM-hypo seem to have an impact on the cholinergic system both in cognitively normal individuals and in patients with vascular cognitive impairment (Liu et al., 2017). Further, the effect of WM-hypo was specific to the cholinergic pathways and did not extend to remaining WM (i.e. WM excluding the cholinergic pathways), when accounting for age.

The random forest models revealed that delayed recall in an episodic memory test (TAVEC delayed recall, both 5 min and 30 min), relies on the integrity of the external capsule pathway. This pathway contains several regions involved in memory such as the frontal cortex and hippocampal structures (Preston and Eichenbaum, 2013). In contrast,

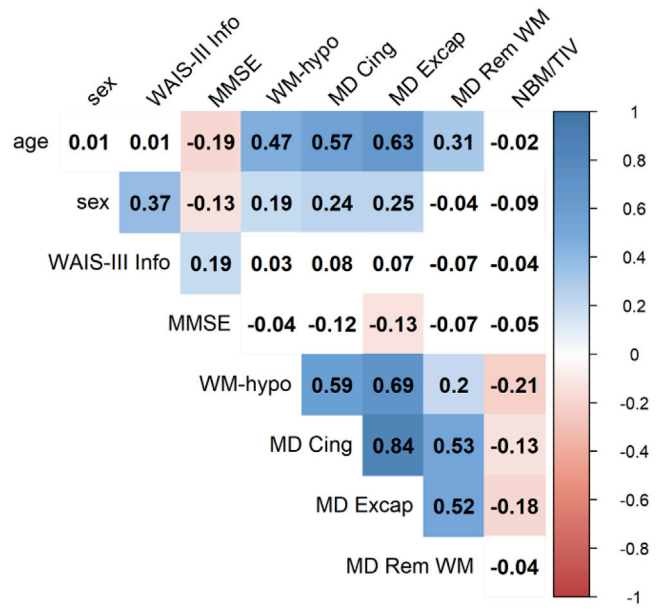

Fig. 5. Correlation matrix for the predictors of the random forest models. Background of significant correlations ($p < 0.05$) was coloured according to the value of the correlation coefficient, otherwise left white. MMSE, Mini-Mental State Examination; sex is coded as 0 for females and 1 for males; MD, mean diffusivity; ExCap, external capsule tract; Cing, cingulum tract; Rem WM, WM excluding cholinergic tracts; WAIS-III Info, Wechsler Adult Intelligence Scale – Third revision Information subtest; WM-hypo, WM hypointensities on T1-weighted images appearing as WM hyperintensities on T2/FLAIR sequences (Wardlaw et al., 2013); NBM/TIV, volume of nucleus basalis scaled by total intracranial volume.

cognitive measures with a stronger attentional component such as PCV – reaction times, as well as TAVEC delayed recall at 30 min, that also involves effortful attention, relied on the integrity of the cingulum. The cingulum involves the posterior cingulate cortex, which is related to attention and memory (Klaassens et al., 2017; Pearson et al., 2011). Of interest, the remaining WM did not contribute to performance in any of the cognitive tests. This finding demonstrates the specificity of the cholinergic pathways to performance in these tests of attention and memory. Older age had an important contribution to all our cognitive variables. However, the contribution of age was lower than that of the integrity of the cholinergic pathways in TAVEC delayed recall (both 5 min and 30 min). These findings suggest that in our cohort of cognitively normal individuals, the contribution of the cholinergic system to cognitive measures is greater and goes beyond the contribution of age in memory tasks that demand effortful attention such as delayed recall. Our findings are thus in agreement with a revisited interpretation of the cholinergic hypothesis of cognitive aging (Dumas and Newhouse, 2011), which proposes that the cholinergic system primarily contributes to effortful attention processes more than memory in cognitively normal individuals. The cholinergic system will thus be especially engaged in attention and memory tasks where the task is difficult and requires effortful attention to achieve good performance (i.e. PCV – reaction time and TAVEC delayed recall, in our study). Our result showing that none of the combinations of variables could predict the TAVEC recognition task further supports this interpretation by indicating that the cholinergic system is not involved in this easier memory task with minimal involvement of attention processes. Although NBM volume plays a key role in AD (Grothe et al., 2012, 2010) and generally in cognitive functioning (Ballinger et al., 2016), it consistently received a very low importance ranking among the other predictors in our random forest models. No association between BF or NBM volume and measures of memory and attention in cognitively normal individuals has been reported in previous studies (Grothe et al., 2016; Lammers et al., 2018, 2016; Wolf et al., 2014). In addition, WM-hypo did not play a strong role in predicting our cognitive measures either. Altogether, our findings point to the integrity of the cholinergic WM pathways as the key factor for performance in attention and memory in our cohort of normal aging. Since both NBM volume and WM-hypo yielded lower contributions in our random forest models, whereas age did yield a high contribution, it is possible that other age-related and subclinical, often mixed, brain pathologies are also contributing to reduced integrity of the cholinergic system (Rahimi and Kovacs, 2014). Using other imaging modalities and biomarkers in the future could help in testing this hypothesis.

A limitation of the current study is that WM pathways that traverse crossing fibres regions may be difficult to track accurately. Several techniques have been proposed to resolve this problem, e.g. multi-tensor fitting, Q-ball imaging, spherical deconvolution, and ball-and-sticks, among other techniques. In the current study, we used a ball-and-sticks model to predict multiple fibre directions in a voxel. While there might exist more advanced techniques, this model shows a good trade-off between model capacity and data quality (Wilkins et al., 2015). Tracking WM pathways through crossing-fibre regions can produce two common types of errors: wrongly connecting brain regions leading to false positives, and omitting existing connections between brain regions leading to false negatives (Dauguet et al., 2007; de Reus and van den Heuvel, 2013). In order to tackle this issue, we performed a combined reconstruction across the whole cohort spanning over 250 individuals that allowed us to set up a robust group threshold - a minimal number of individual cases who share a connection before it was included in the model. A high group threshold requires the connection to be present in a high number of individuals, which has previously successfully eliminated false positives (Watson et al., 2019; Wiseman et al., 2018). On the other hand, a low group threshold allows for unique tracks and ensures a low false-negative rate. In this study, we followed and adapted the methods from de Reus and van den Heuvel (2013) and Liu et al. (2017). Constraining fibre tracking by using hypothesis-driven *a priori* information also helps to reduce the amount of false-positive errors in our cingulum and external capsule models. However, this may happen at the expense of slightly increasing the amount of false-negative errors, i.e. exclusion of areas not considered in *a priori* knowledge. For this reason, we performed an unconstrained tractography model that was able to include areas of the posterior cingulate and superior medial parietal and frontal lobes with potential to be truly cholinergic (Fritz et al., 2019; Selden et al., 1998). Hence, we encourage further studies to substantiate our findings from the unconstrained model. Future advances and refinement of tractography methods are also expected to minimise the rate of false positives and false negatives. Furthermore, we favoured the MD index to other diffusion indices such as fractional anisotropy for its reduced susceptibility to the crossing-fibre problem. We investigated the NBM, which provides the major cholinergic input to cortical and subcortical areas, and has a strong involvement in cognition. However, investigating the fornix, which contains cholinergic projections from the septal nuclei to the hippocampus is warranted for future studies, due to its involvement in episodic verbal memory in cognitively healthy individuals. Investigating other cognitive functions previously linked to the cholinergic system, e.g. cognitive control, is also warranted for future studies. Random forest regression with conditional inference trees is able to handle multicollinearity to some degree, but it might lead to an underestimation of the contribution of multicollinear variables. The association among the predictors of the random forest models can be appreciated in Fig. 5. Finally, previous studies using the cholinergic pathways hyperintensities scale (CHIPS) demonstrated that WM-hypo in presumably cholinergic WM pathways have an impact on cognition in patients with AD and different clinical conditions including probable vascular dementia, vascular cognitive impairment no dementia, and subcortical ischemic vasculopathy (Jaswal et al., 2018; Kim et al., 2013; Swartz et al., 2003). Compared to the CHIPS, our current tractography method gives direct and richer information on the integrity of the cholinergic system but the WM-hypo quantification method lacks regional information. Therefore,

in the future, we will develop regional applications of our current approach.

5. Conclusions

In conclusion, using the proposed pipeline we modelled human WM tracts in a manner that closely resembles cholinergic pathways depicted in post-mortem findings (Selden et al., 1998) and a previous smaller sample DTI-tractography study (Liu et al., 2017). We show that lower integrity of these cholinergic pathways along with age are strong contributors to performance in tests of attention and memory in our cohort of cognitively normal middle-aged and older individuals. Future studies are needed to test whether the developed method could be used as an *in vivo* marker of the human cholinergic system in both cognitively normal and pathological populations. If further validated, we hope that the current method and complementary approaches such as BF functional connectivity in rs-fMRI data (Fritz et al., 2019) will provide new *in vivo* opportunities to re-evaluate the cholinergic hypothesis of cognitive aging.

Declaration of competing interest

None.

CRediT authorship contribution statement

Milan Nemy: Conceptualization, Methodology, Formal analysis, Writing - original draft, Visualization, Software. **Nira Cedres:** Conceptualization, Writing - original draft, Data curation, Investigation. **Michel J. Grothe:** Resources, Writing - review & editing. **J-Sebastian Muehlboeck:** Software, Writing - review & editing. **Olof Lindberg:** Data curation, Writing - review & editing. **Zuzana Nedelska:** Conceptualization, Writing - review & editing. **Olga Stepankova:** Resources, Writing - review & editing. **Lenka Vyslouzilova:** Resources, Writing - review & editing. **Maria Eriksdotter:** Writing - review & editing, Funding acquisition. **José Barroso:** Resources, Writing - review & editing, Funding acquisition. **Stefan Teipel:** Resources, Writing - review & editing. **Eric Westman:** Funding acquisition, Resources, Writing - review & editing. **Daniel Ferreira:** Conceptualization, Methodology, Investigation, Writing - original draft, Writing - review & editing, Supervision, Project administration, Funding acquisition.

Acknowledgements

This research was supported by the *Fundación Canaria Dr. Manuel Morales* (calls 2012, 2014 and 2017); *Fundación Cajacanarias*; the Swedish Foundation for Strategic Research (SSF), the Strategic Research Programme in Neuroscience at Karolinska Institutet (StratNeuro), the Swedish Research Council (VR), the Åke Wiberg foundation, Hjärnfonden, Alzheimerfonden, Demensfonden Stiftelsen Olle Engkvist Byggmästare, Birgitta och Sten Westerberg, Ålderssjukdomar, Gun and Bertil Stohnes, Sigurd och Elsa Goljes Minne, Gamla Tjänarinnor, Karolinska Institutet Forskningstiftelse, Demensförbundet, the Grant Agency of the Czech Technical University in Prague, grant No. SGS19/111/OHK4/2T/13, the Czech Alzheimer Foundation, and the IBRO-ISN fellowship 2018. The funders of the study had no role in the study design nor the collection, analysis, and interpretation of data, writing of the report, or decision to submit the manuscript for publication. The authors would like to thank Dr. Diaz-Flores Varela (Hospital Universitario de Canarias, Tenerife, Spain) for his collaboration in the inspection of magnetic resonance images for inclusion criteria; Dr. Antonio Rodríguez for providing access to participants and helpful assistance; and *Servicio de Resonancia Magnética para Investigaciones Biomédicas del SEGAI* (University of La Laguna, Spain). Data used in preparation of this article is part of the GENIC-database (Group of Neuropsychological Studies of the Canary Islands, University of La Laguna, Spain. Principal investigator: Professor José Barroso. Contact: Dr. Daniel Ferreira, daniel.ferreira.padilla@ki.se). The following collaborators contributed to the GENIC-database but did not participate in analysis or writing of this report (in alphabetic order by family name): Rut Correia, Patricia Diaz, Aida Figueroa, Nerea Figueroa, Eloy García, Lissett González, Teodoro González, Zaira González, Cathaysa Hernández, Edith Hernández, Nira Jiménez, Judith López, Cándida Lozano, María Antonieta Nieto, María Sabucedo, Elena Sirumal, Marta Suárez, Manuel Urbano, and Pedro Velasco.

References

Acosta-Cabronero, J., Williams, G.B., Pengas, G., Nestor, P.J., 2010. Absolute diffusivities define the landscape of white matter degeneration in Alzheimer's disease. Brain 133, 529–539. https://doi.org/10.1093/brain/awp257.

Andersson, J.L.R., Sotiropoulos, S.N., 2016. An integrated approach to correction for off-resonance effects and subject movement in diffusion MR imaging. Neuroimage 125, 1063–1078. https://doi.org/10.1016/j.neuroimage.2015.10.019.

Avants, B.B., Epstein, C.L., Grossman, M., Gee, J.C., 2008. Symmetric diffeomorphic image registration with cross-correlation: evaluating automated labeling of elderly and neurodegenerative brain. Med. Image Anal. 12, 26–41. https://doi.org/10.1016/j.media.2007.06.004.

Ballinger, E.C., Ananth, M., Talmage, D.A., Role, L.W., 2016. Basal forebrain cholinergic circuits and signaling in cognition and cognitive decline. Neuron 91, 1199–1218. https://doi.org/10.1016/j.neuron.2016.09.006.

Bartus, R.T., Dean, R.L., Beer, B., Lippa, A.S., 1982. The cholinergic hypothesis of geriatric memory dysfunction. Science 217, 408–414. https://doi.org/10.1126/SCIENCE.7046051.

Beck, A.T., Ward, C.H., Mendelson, M., Mock, J., Erbaugh, J., 1961. An inventory for measuring depression. Arch. Gen. Psychiatr. 4, 561–571.

Behrens, T.E.J., Berg, H.J., Jbabdi, S., Rushworth, M.F.S., Woolrich, M.W., 2007. Probabilistic diffusion tractography with multiple fibre orientations: what can we gain? Neuroimage. https://doi.org/10.1016/j.neuroimage.2006.09.018.

Benedet Mj, A.M., 1998. TAVEC: Test de Aprendizaje Verbal España-Complutense. TEA, Madrid.

Blessed, G., Tomlinson, B.E., Roth, M., 1968. The association between quantitative measures of dementia and of senile change in the cerebral grey matter of elderly subjects. Br. J. Psychiatry 114, 797–811. https://doi.org/10.1192/bjp.114.512.797.

Brands, A.M.A., Kessels, R.P.C., Hoogma, R.P.L.M., Henselmans, J.M.L., Van Der Beek Boter, J.W., Kappelle, L.J., De Haan, E.H.F., Biessels, G.J., 2006. Cognitive performance, psychological well-being, and brain magnetic resonance imaging in older patients with type 1 diabetes. Diabetes 55, 1800–1806. https://doi.org/10.2337/db05-1226.

Breiman, L., 2001. Random forests. Mach. Learn. 45, 5–32. https://doi.org/10.1023/A:1010933404324.

Breiman, L., 1996. Bagging predictions. Mach. Learn. 24, 123–140. https://doi.org/10.1023/A:1018054314350.

Buckner, R.L., Head, D., Parker, J., Fotenos, A.F., Marcus, D., Morris, J.C., Snyder, A.Z., 2004. A unified approach for morphometric and functional data analysis in young, old, and demented adults using automated atlas-based head size normalization: reliability and validation against manual measurement of total intracranial volume. Neuroimage 23, 724–738. https://doi.org/10.1016/J.NEUROIMAGE.2004.06.018.

Butler, T., Blackmon, K., Zaborszky, L., Wang, X., DuBois, J., Carlson, C., Barr, W.B., French, J., Devinsky, O., Kuzniecky, R., Halgren, E., Thesen, T., 2012. Volume of the human septal forebrain region is a predictor of source memory accuracy. J. Int. Neuropsychol. Soc. 18, 157–161. https://doi.org/10.1017/s1355617711001421.

Cedres, N., Ferreira, D., Machado, A., Shams, S., Sacuiu, S., Waern, M., Wahlund, L.-O., Zettergren, A., Kern, S., Skoog, I., Westman, E., 2020. Predicting Fazekas scores from automatic segmentations of white matter signal abnormalities. Aging 12, 894–901. https://doi.org/10.18632/aging.102662.

Cedres, N., Machado, A., Molina, Y., Diaz-Galvan, P., Hernández-Cabrera, J.A., Barroso, J., Westman, E., Ferreira, D., 2019. Subjective cognitive decline below and above the age of 60: a multivariate study on neuroimaging, cognitive, clinical, and demographic measures. J. Alzheim. Dis. 68, 295–309. https://doi.org/10.3233/JAD-180720.

Dauguet, J., Peled, S., Berezovskii, V., Delzescaux, T., Warfield, S.K., Born, R., Westin, C.F., 2007. Comparison of fiber tracts derived from in-vivo DTI tractography with 3D histological neural tract tracer reconstruction on a macaque brain. Neuroimage 37, 530–538. https://doi.org/10.1016/j.neuroimage.2007.04.067.

de Reus, M.A., van den Heuvel, M.P., 2013. Estimating false positives and negatives in brain networks. Neuroimage 70, 402–409. https://doi.org/10.1016/j.neuroimage.2012.12.066.

Drachman, D.A., Leavitt, J., 1974. Human memory and the cholinergic system: a relationship to aging? Arch. Neurol. 30, 113–121. https://doi.org/10.1001/archneur.1974.00490320001001.

Dumas, J.A., Newhouse, P.A., 2011. The cholinergic hypothesis of cognitive aging revisited again: cholinergic functional compensation. Pharmacol. Biochem. Behav. 99, 254–261. https://doi.org/10.1016/j.pbb.2011.02.022.

Ferreira, D., Correia, R., Nieto, A., Machado, A., Molina, Y., Barroso, J., 2015. Cognitive decline before the age of 50 can be detected with sensitive cognitive measures. Psicothema 27, 216–222. https://doi.org/10.7334/psicothema2014.192.

Ferreira, D., Machado, A., Molina, Y., Nieto, A., Correia, R., Westman, E., Barroso, J., 2017. Cognitive variability during middle-age: possible association with neurodegeneration and cognitive reserve. Front. Aging Neurosci. 9, 188. https://doi.org/10.3389/fnagi.2017.00188.

Ferreira, D., Molina, Y., Machado, A., Westman, E., Wahlund, L.O., Nieto, A., Correia, R., Junqué, C., Díaz-Flores, L., Barroso, J., 2014. Cognitive decline is mediated by gray matter changes during middle age. Neurobiol. Aging 35, 1086–1094. https://doi.org/10.1016/j.neurobiolaging.2013.10.095.

Fischl, B., Salat, D.H., Busa, E., Albert, M., Dieterich, M., Haselgrove, C., van der Kouwe, A., Killiany, R., Kennedy, D., Klaveness, S., Montillo, A., Makris, N., Rosen, B., Dale, A.M., 2002. Whole brain segmentation: automated labeling of neuroanatomical structures in the human brain. Neuron 33, 341–355. https://doi.org/10.1016/S0896-6273(02)00569-X.

Folstein, M.F., Folstein, S.E., McHugh, P.R., 1975. "Mini-mental state". A practical method for grading the cognitive state of patients for the clinician. J. Psychiatr. Res. 12, 189–198. https://doi.org/10.1016/0022-3956(75)90026-6.

Fritz, H.C.J., Ray, N., Dyrba, M., Sorg, C., Teipel, S., Grothe, M.J., 2019. The corticotopic organization of the human basal forebrain as revealed by regionally selective functional connectivity profiles. Hum. Brain Mapp. 40, 868–878. https://doi.org/10.1002/hbm.24417.

Grothe, M., Heinsen, H., Teipel, S., 2013. Longitudinal measures of cholinergic forebrain atrophy in the transition from healthy aging to Alzheimer's disease. Neurobiol. Aging 34, 1210–1220. https://doi.org/10.1016/j.neurobiolaging.2012.10.018.

Grothe, M., Heinsen, H., Teipel, S.J., 2012. Atrophy of the cholinergic basal forebrain over the adult age range and in early stages of Alzheimer's disease. Biol. Psychiatr. 71, 805–813. https://doi.org/10.1016/j.biopsych.2011.06.019.

Grothe, M., Zaborszky, L., Atienza, M., Gil-Neciga, E., Rodriguez-Romero, R., Teipel, S.J., Amunts, K., Suarez-Gonzalez, A., Cantero, J.L., 2010. Reduction of basal forebrain cholinergic system parallels cognitive impairment in patients at high risk of developing alzheimer's disease. Cerebr. Cortex 20, 1685–1695. https://doi.org/10.1093/cercor/bhp232.

Grothe, M.J., Heinsen, H., Amaro, E., Grinberg, L.T., Teipel, S.J., 2016. Cognitive correlates of basal forebrain atrophy and associated cortical hypometabolism in mild cognitive impairment. Cerebr. Cortex 26, 2411–2426. https://doi.org/10.1093/cercor/bhv062.

Gunning-Dixon, F.M., Brickman, A.M., Cheng, J.C., Alexopoulos, G.S., 2009. Aging of cerebral white matter: a review of MRI findings. Int. J. Geriatr. Psychiatr. 24, 109–117. https://doi.org/10.1002/gps.2087.

Gustavsson, A.-M., Stomrud, E., Abul-Kasim, K., Minthon, L., Nilsson, P.M., Hansson, O., Nägga, K., 2015. Cerebral microbleeds and white matter hyperintensities in cognitively healthy elderly: a cross-sectional cohort study evaluating the effect of arterial stiffness. Cerebrovasc. Dis. Extra 5, 41–51. https://doi.org/10.1159/000377710.

Habes, M., Erus, G., Toledo, J.B., Zhang, T., Bryan, N., Launer, L.J., Rosseel, Y., Janowitz, D., Doshi, J., Van der Auwera, S., von Sarnowski, B., Hegenscheid, K., Hosten, N., Homuth, G., Völzke, H., Schminke, U., Hoffmann, W., Grabe, H.J., Davatzikos, C., 2016. White matter hyperintensities and imaging patterns of brain ageing in the general population. Brain 139, 1164–1179. https://doi.org/10.1093/brain/aww008.

Hawkins, K.A., Emadi, N., Pearlson, G.D., Winkler, A.M., Taylor, B., Dulipsingh, L., King, D., Pittman, B., Blank, K., 2017. Hyperinsulinemia and elevated systolic blood pressure independently predict white matter hyperintensities with associated cognitive decrement in the middle-aged offspring of dementia patients. Metab. Brain Dis. 32, 849–857. https://doi.org/10.1007/s11011-017-9980-9.

Jaswal, G., Swardfager, W., Gao, F.-Q., Nestor, S.M., Ganda, A., Cogo-Moreira, H., Sahlas, D.J., Stuss, D.T., Moody, A., Black, S.E., 2018. Reduced substantia innominata volume mediates contributions of microvascular and macrovascular disease to cognitive deficits in Alzheimer's disease. Neurobiol. Aging 66, 23–31. https://doi.org/10.1016/j.neurobiolaging.2018.01.025.

Jenkinson, M., Beckmann, C.F., Behrens, T.E.J., Woolrich, M.W., Smith, S.M., 2012. FSL. Neuroimage 62, 782–790. https://doi.org/10.1016/j.neuroimage.2011.09.015.

Jenkinson, M., Pechaud, M., Smith, S., 2005. BET2: MR-based estimation of brain, skull and scalp surfaces. In: Eleventh Annual Meeting of the Organization for Human Brain Mapping, vol. 17, p. 167.

Kilimann, I., Grothe, M., Heinsen, H., Alho, E.J.L., Grinberg, L., Amaro, E., Dos Santos, G.A.B., Da Silva, R.E., Mitchell, A.J., Frisoni, G.B., Bokde, A.L.W., Fellgiebel, A., Filippi, M., Hampel, H., Klöppel, S., Teipel, S.J., 2014. Subregional basal forebrain atrophy in alzheimer's disease: a multicenter study. J. Alzheim. Dis. 40, 687–700. https://doi.org/10.3233/JAD-132345.

Kim, H.J., Moon, W.J., Han, S.H., 2013. Differential cholinergic pathway involvement in alzheimer's disease and subcortical ischemic vascular dementia. J. Alzheim. Dis. 35, 129–136. https://doi.org/10.3233/JAD-122320.

Klaassens, B.L., van Gerven, J.M.A., van der Grond, J., de Vos, F., Möller, C., Rombouts, S.A.R.B., 2017. Diminished posterior precuneus connectivity with the default mode network differentiates normal aging from Alzheimer's Disease. Front. Aging Neurosci. 9 https://doi.org/10.3389/fnagi.2017.00097.

Lammers, F., Borchers, F., Feinkohl, I., Hendrikse, J., Kant, I.M.J., Kozma, P., Pischon, T., Slooter, A.J.C., Spies, C., van Montfort, S.J.T., Zacharias, N., Zaborszky, L., Winterer, G., 2018. Basal forebrain cholinergic system volume is associated with general cognitive ability in the elderly. Neuropsychologia 119, 145–156. https://doi.org/10.1016/j.neuropsychologia.2018.08.005.

Lammers, F., Mobascher, A., Musso, F., Shah, N.J., Warbrick, T., Zaborszky, L., Winterer, G., 2016. Effects of Ncl. Basalis Meynert volume on the Trail-Making-Test are restricted to the left hemisphere. Brain Behav. 6, 1–9. https://doi.org/10.1002/brb3.421.

Leritz, E.C., Shepel, J., Williams, V.J., Lipsitz, L.A., Mcglinchey, R.E., Milberg, W.P., Salat, D.H., 2014. Associations between T1 white matter lesion volume and regional white matter microstructure in aging. Hum. Brain Mapp. 35, 1085–1100. https://doi.org/10.1002/hbm.22236.

Li, X., Li, T.Q., Andreasen, N., Wiberg, M.K., Westman, E., Wahlund, L.O., 2014. The association between biomarkers in cerebrospinal fluid and structural changes in the brain in patients with Alzheimer's disease. J. Intern. Med. 275, 418–427. https://doi.org/10.1111/joim.12164.

Li, X., Westman, E., Ståhlbom, A.K., Thordardottir, S., Almkvist, O., Blennow, K., Wahlund, L.O., Graff, C., 2015. White matter changes in familial Alzheimer's disease. J. Intern. Med. 278, 211–218. https://doi.org/10.1111/joim.12352.

Liu, Q., Zhu, Z., Teipel, S.J., Yang, J., Xing, Y., Tang, Y., Jia, J., 2017. White matter damage in the cholinergic system contributes to cognitive impairment in subcortical vascular cognitive impairment, no dementia. Front. Aging Neurosci. 9, 47. https://doi.org/10.3389/fnagi.2017.00047.

Machado, A., Barroso, J., Molina, Y., Nieto, A., Díaz-Flores, L., Westman, E., Ferreira, D., 2018. Proposal for a hierarchical, multidimensional, and multivariate approach to investigate cognitive aging. Neurobiol. Aging 71, 179–188. https://doi.org/10.1016/J.NEUROBIOLAGING.2018.07.017.

Mesulam, M.M., 2013. Cholinergic circuitry of the human nucleus basalis and its fate in Alzheimer's disease. J. Comp. Neurol. https://doi.org/10.1002/cne.23415.

Mesulam, M.M., Mufson, E.J., Levey, A.I., Wainer, B.H., 1983. Cholinergic innervation of cortex by the basal forebrain: cytochemistry and cortical connections of the septal area, diagonal band nuclei, nucleus basalis (Substantia innominata), and hypothalamus in the rhesus monkey. J. Comp. Neurol. 214, 170–197. https://doi.org/10.1002/cne.902140206.

Mesulam, M.M., Mufson, E.J., Wainer, B.H., 1986. Three-dimensional representation and cortical projection topography of the nucleus basalis (Ch4) in the macaque: concurrent demonstration of choline acetyltransferase and retrograde transport with a stabilized tetramethylbenzidine method for horseradish p. Brain Res. 367, 301–308. https://doi.org/10.1016/0006-8993(86)91607-0.

Mesulam, M.M., Van Hoesen, G.W., 1976. Acetylcholinesterase-rich projections from the basal forebrain of the rhesus monkey to neocortex. Brain Res. 109, 152–157. https://doi.org/10.1016/0006-8993(76)90385-1.

Mori, S., Wakana, S., Van Zijl, P.C., Nagae-Poetscher, L., 2005. MRI Atlas of Human White Matter. Elsevier, Amsterdam.

Nunley, K.A., Ryan, C.M., Orchard, T.J., Aizenstein, H.J., Jennings, J.R., Ryan, J., Zgibor, J.C., Boudreau, R.M., Costacou, T., Maynard, J.D., Miller, R.G., Rosano, C., 2015. White matter hyperintensities in middle-aged adults with childhood-onset type 1 diabetes. Neurology 84, 2062–2069. https://doi.org/10.1212/WNL.0000000000001582.

Patenaude, B., Smith, S.M., Kennedy, D.N., Jenkinson, M., 2011. A Bayesian model of shape and appearance for subcortical brain segmentation. Neuroimage 56, 907–922. https://doi.org/10.1016/j.neuroimage.2011.02.046.

Pearson, J.M., Heilbronner, S.R., Barack, D.L., Hayden, B.Y., Platt, M.L., 2011. Posterior cingulate cortex: adapting behavior to a changing world. Trends Cognit. Sci. https://doi.org/10.1016/j.tics.2011.02.002.

Pfeffer, R.I., Kurosaki, T.T., Harrah, C.H., Chance, J.M., Filos, S., 1982. Measurement of functional activities in older adults in the community. J. Gerontol. 37, 323–329.

Preston, A.R., Eichenbaum, H., 2013. Interplay of hippocampus and prefrontal cortex in memory. Curr. Biol. https://doi.org/10.1016/j.cub.2013.05.041.

Rahimi, J., Kovacs, G.G., 2014. Prevalence of mixed pathologies in the aging brain. Alzheimer's Res. Ther. 6 https://doi.org/10.1186/s13195-014-0082-1.

Raz, N., Yang, Y., Dahle, C.L., Land, S., 2012. Volume of white matter hyperintensities in healthy adults: contribution of age, vascular risk factors, and inflammation-related genetic variants. Biochim. Biophys. Acta - Mol. Basis Dis. 1822, 361–369. https://doi.org/10.1016/j.bbadis.2011.08.007.

Salat, D.H., Tuch, D.S., van der Kouwe, A.J.W., Greve, D.N., Pappu, V., Lee, S.Y., Hevelone, N.D., Zaleta, A.K., Growdon, J.H., Corkin, S., Fischl, B., Rosas, H.D., 2010. White matter pathology isolates the hippocampal formation in Alzheimer's disease. Neurobiol. Aging 31, 244–256. https://doi.org/10.1016/j.neurobiolaging.2008.03.013.

Schuhfried, G., 1992. Vienna Reaction Unit (Manual). Schuhfried Ges. mbH, Mödling, Austria.

Selden, N.R., Gitelman, D.R., Salamon-Murayama, N., Parrish, T.B., Mesulam, M.M., 1998. Trajectories of cholinergic pathways within the cerebral hemispheres of the human brain. Brain J. Neurol. 121, 2249–2257. https://doi.org/10.1093/brain/121.12.2249.

Simmons, A., Westman, E., Muehlboeck, S., Mecocci, P., Vellas, B., Tsolaki, M., Kłoszewska, I., Wahlund, L.-O., Soininen, H., Lovestone, S., Evans, A., Spenger, C., 2009. MRI measures of alzheimer's disease and the AddNeuroMed study. Ann. N. Y. Acad. Sci. 1180, 47–55. https://doi.org/10.1111/j.1749-6632.2009.05063.x.

Strobl, C., Boulesteix, A.L., Zeileis, A., Hothorn, T., 2007. Bias in random forest variable importance measures: illustrations, sources and a solution. BMC Bioinf. 8 https://doi.org/10.1186/1471-2105-8-25.

Stroop, J.R., 1935. Studies of interference in serial verbal reactions. J. Exp. Psychol. 18, 643–662. https://doi.org/10.1037/h0054651.

Swartz, R.H., Sahlas, D.J., Black, S.E., 2003. Strategic involvement of cholinergic pathways and executive dysfunction: does location of white matter signal hyperintensities matter? J. Stroke Cerebrovasc. Dis. 12, 29–36. https://doi.org/10.1053/JSCD.2003.5.

Teipel, S., Heinsen, H., Amaro, E., Grinberg, L.T., Krause, B., Grothe, M., Alzheimer's Disease Neuroimaging Initiative, M., 2014. Cholinergic basal forebrain atrophy predicts amyloid burden in Alzheimer's disease. Neurobiol. Aging 35, 482–491. https://doi.org/10.1016/j.neurobiolaging.2013.09.029.

Teipel, S.J., Flatz, W.H., Heinsen, H., Bokde, A.L.W., Schoenberg, S.O., Stöckel, S., Dietrich, O., Reiser, M.F., Möller, H.J., Hampel, H., 2005. Measurement of basal forebrain atrophy in Alzheimer's disease using MRI. Brain 128, 2626–2644. https://doi.org/10.1093/brain/awh589.

Teipel, S.J., Meindl, T., Grinberg, L., Grothe, M., Cantero, J.L., Reiser, M.F., Möller, H.-J., Heinsen, H., Hampel, H., 2011. The cholinergic system in mild cognitive impairment and Alzheimer's disease: an in vivo MRI and DTI study. Hum. Brain Mapp. 32, 1349–1362. https://doi.org/10.1002/hbm.21111.

Wardlaw, J.M., Smith, E.E., Biessels, G.J., Cordonnier, C., Fazekas, F., Frayne, R., Lindley, R.I., O'Brien, J.T., Barkhof, F., Benavente, O.R., Black, S.E., Brayne, C., Breteler, M., Chabriat, H., DeCarli, C., de Leeuw, F.E., Doubal, F., Duering, M., Fox, N.C., Greenberg, S., Hachinski, V., Kilimann, I., Mok, V., Oostenbrugge, R. van, Pantoni, L., Speck, O., Stephan, B.C.M., Teipel, S., Viswanathan, A., Werring, D., Chen, C., Smith, C., van Buchem, M., Norrving, B., Gorelick, P.B., Dichgans, M., 2013. Neuroimaging standards for research into small vessel disease and its contribution to ageing and neurodegeneration. Lancet Neurol. https://doi.org/10.1016/S1474-4422(13)70124-8.

Watson, C.G., DeMaster, D., Ewing-Cobbs, L., 2019. Graph theory analysis of DTI tractography in children with traumatic injury. NeuroImage Clin. 21, 101673. https://doi.org/10.1016/J.NICL.2019.101673.

Wechsler, D., 1997. WMS-III: Wechsler Memory Scale Administration and Scoring Manual. Psychological Corporation, San Antonio.

Wilkins, B., Lee, N., Gajawelli, N., Law, M., Leporé, N., 2015. Fiber estimation and tractography in diffusion MRI: development of simulated brain images and comparison of multi-fiber analysis methods at clinical b-values HHS Public Access. Neuroimage 109, 341–356. https://doi.org/10.1016/j.neuroimage.2014.12.060.

Wiseman, S.J., Booth, T., Ritchie, S.J., Cox, S.R., Muñoz Maniega, S., Valdés Hernández, M.D.C., Dickie, D.A., Royle, N.A., Starr, J.M., Deary, I.J., Wardlaw, J.M., Bastin, M.E., 2018. Cognitive abilities, brain white matter hyperintensity volume, and structural network connectivity in older age. Hum. Brain Mapp. 39, 622–632. https://doi.org/10.1002/hbm.23857.

Wolf, D., Grothe, M., Fischer, F.U., Heinsen, H., Kilimann, I., Teipel, S., Fellgiebel, A., 2014. Association of basal forebrain volumes and cognition in normal aging. Neuropsychologia 53, 54–63. https://doi.org/10.1016/j.neuropsychologia.2013.11.002.

Woolf, N.J., 1991. Cholinergic systems in mammalian brain and spinal cord. Prog. Neurobiol. 37, 475–524. https://doi.org/10.1016/0301-0082(91)90006-M.

Yang, T., Sun, Y., Lu, Z., Leak, R.K., Zhang, F., 2017. The impact of cerebrovascular aging on vascular cognitive impairment and dementia. Ageing Res. Rev. 34, 15. https://doi.org/10.1016/J.ARR.2016.09.007.

Yesavage, J.A., Sheikh, J.I., 1986. Geriatric depression scale (GDS). Clin. Gerontol. 5, 165–173. https://doi.org/10.1300/J018v05n01_09.

Zaborszky, L., Hoemke, L., Mohlberg, H., Schleicher, A., Amunts, K., Zilles, K., 2008. Stereotaxic probabilistic maps of the magnocellular cell groups in human basal forebrain. Neuroimage 42, 1127–1141. https://doi.org/10.1016/j.neuroimage.2008.05.055.

Zhang, B., Xu, Y., Zhu, B., Kantarci, K., 2014. The role of diffusion tensor imaging in detecting microstructural changes in prodromal Alzheimer's disease. CNS Neurosci. Ther. 20, 3–9. https://doi.org/10.1111/cns.12166.

Zhang, Y., Brady, M., Smith, S., 2001. Segmentation of brain MR images through a hidden Markov random field model and the expectation-maximization algorithm. IEEE Trans. Med. Imag. 20, 45–57. https://doi.org/10.1109/42.906424.